3D printing of lignin-based polymeric composites obtained using liquid crystal display as a vat photopolymerization technique

Research Article

Received: 16 January 2025 Revised: 14 April 2025 Published online in Wiley Online Library: 29 May 2025

(wileyonlinelibrary.com) DOI 10.1002/pi.6783

3D printing of lignin-based polymeric composites obtained using liquid crystal display as a vat photopolymerization technique

Giovanna Colucci,[a,b*] Francesca Sacchi,[a,b] Federica Bondioli[a,b] and Massimo Messori[a,b]

Abstract

The present work aims to improve the sustainability of polymers and may pave the way for the development through 3D technologies of innovative composites useful for many industries. It highlights the preparation of lignin-based composites by adding lignin to an acrylate epoxidized soybean oil (AESO) resin using a liquid crystal display (LCD) 3D printer. The formulations were obtained by adding tetrahydrofurfuryl acrylate (THFA) as reactive diluent to the AESO matrix as the starting reference system. Then, lignin-based composites were obtained by dispersing lignin at different concentrations within the AESO-THFA resin. The viscosity and printability of the photocurable formulations were first studied because they play a key role in a vat photopolymerization process. Several 3D printed parts were successfully realized via LCD exhibiting high resolution and accuracy and well-detailed geometries. SEM analyses revealed that lignin particles were homogeneously dispersed within the crosslinked AESO-based network. The thermal and mechanical properties of the photocured lignin-based composites were tested by TGA, dynamic mechanical thermal analysis and tensile tests, underlining that the presence of lignin led to a decrease of the elastic modulus and tensile strength, and a slight increase of the glass transition temperature, leaving the thermal stability unchanged. The incorporation of lignin into an AESO polymer network can significantly improve the sustainability of polymers designing and printing innovative lignin-based composites useful for many industrial fields.

Supporting information may be found in the online version of this article.

Keywords: lignin; polymer composites; vat photopolymerization; 3D printing; liquid crystal display (LCD)

HIGHLIGHTS

- Lignin-based composites were prepared by LCD vat photopolymerization.
- 3D printed objects were realized by adding lignin to AESO photocurable resin.
- The parts show increasing complexity structures and high level of definition.
- Thermal, morphological and mechanical properties were widely studied.

INTRODUCTION

The need for sustainable alternatives to traditional polymers deriving from fossil-based sources has been encouraging academic and industrial researchers to develop and investigate bio-based polymers and polymer composites generating innovative environmentally sustainable and economically competitive polymeric materials viable for many manufacturing processes and application fields. In this scenario, additive manufacturing (AM) can guarantee a significant reduction of raw material, energy consumption and waste generation during the processing, also reducing cost and time.[1–3] AM can offer higher freedom and flexibility of design, enabling the manufacture of a wide number of structures and geometries. Moreover, AM can ensure the possibility of realizing prototypes and of achieving lightweight components with high dimensional accuracy, reducing the high costs for the realization of non-standard geometries and moulds.[1,2] AM has seen an exponential development and an implementation in many industrial fields, such as prototyping for aerospace and motorsports, spare parts for the automotive sector and customized tools for the biomedical sector.[3,4]

Several 3D printing technologies are available for polymeric feedstocks, including material extrusion, powder bed fusion,

* *Correspondence to: G Colucci, Politecnico di Torino, Dipartimento di Scienza Applicata e Tecnologia (DISAT), Torino, Italy. E-mail: giovanna.colucci@polito.it*

a *Politecnico di Torino, Dipartimento di Scienza Applicata e Tecnologia (DISAT), Torino, Italy*

b *Consorzio Interuniversitario Nazionale per la Scienza e Tecnologia dei Materiali (INSTM), Florence, Italy*

material jetting and vat photopolymerization (VP).[3–6] VP technologies, including stereolithography, digital light processing (DLP) and liquid crystal display (LCD), are based on a photopolymerization process that requires a photoinitiator and reactive functional monomers or oligomers suitable for chain-growth polymerization reactions. A UV–visible light source promotes the photopolymerization of the liquid monomers into a solid 3D network. It is a very complex process which involves simultaneous control of the resin properties, in terms of rheology, chemistry and processability, to provide photocured thermoset objects.[7–9] VP 3D printers generally present two main different configurations. In the first layout, the light source is above the liquid resin bath and each layer is printed on top of the previous one while the build platform moves down into the vat.[9] In the second choice, the light source is below the resin bath. The desired object is obtained layer by layer between the bottom of the bath and the build platform. A successive step is required to remove the cured object from the bottom of the vat. In this last case, the resin must have a sufficiently low viscosity to flow into the vat by moving the build platform.[9] Currently, non-biodegradable and non-bio-based photopolymers are mainly used for VP 3D printing. To overcome this limitation and decrease the environmental impact, research is exploring the possibility of using different types of bio-derived photopolymers, like vegetable oils, which have great potential in developing new classes of polymers.[10,11] However, the mechanical properties of the printed parts were generally very poor. For this reason, the production of composite materials compatible with existing 3D printers has gained considerable attention in recent years. Fillers can be added to the vegetable oils with the aim of enhancing the mechanical properties and of extending the possible application fields of the final 3D printed parts. Many studies have been reported in the literature on the preparation of composites for 3D printing applications by the addition of bio-based and renewable fillers or fibres, from different sources or waste, to a polymeric photocurable resin, and prospects for the development of materials with final added values, in terms of mechanical and thermal properties, and biocompatibility have been defined.[12,13] Some authors prepared crosslinked polymers by 3D printing using vanillin derivatives, such as vanillin dimethacrylate and vanillin diacrylate with values of crosslinking density, thermal stability and mechanical properties higher than those of commercial petroleum-derived materials.[14,15] Moreover, methacrylate carboxymethyl cellulose or keratin were used as bio-based fillers for 3D printing of different types of biocompatible hydrogels. Novel bio-based photocurable inks were developed for DLP 3D printing to obtain hydrogels and scaffolds with excellent swelling ability, cytocompatibility and mechanical properties, useful for biomedical applications.[16,17] Bio-based polymeric composites were also prepared by 3D printing by dispersing fillers coming from agro-wastes within a thermoset resin with improved final properties.[18,19] Finally, the development of printable and biocompatible silk fibroin bio-inks for DLP 3D printing that can be used for tissue and organ engineering in the biomedical field was also reported.[20]

Among bio-based polymers, lignin-based polymers have attracted great attention for 3D printing in the last few years.[21] This is because lignin is the second most abundant biopolymer on Earth and because it is available as a natural reinforcing filler for polymer matrices.[21–25] In this context, 3D printing can represent a promising way to add value to lignin with the purpose of preparing sustainable lignin-based polymeric composites, valorising the use of this kind of filler. Some research has shown that lignin or lignin-based biopolymers and their derivatives can represent a new source of materials with great potential for the VP printing process. In fact, they can be proficiently used to develop photopolymers for stereolithography, DLP and material jetting 3D printing, giving rise to the development of alternative photopolymer materials with improved properties compared with traditional materials.[26–31]

In the present paper, lignin-based composites were prepared by adding different amounts of lignin within a soybean-oil-based resin by using, for the first time to the authors' knowledge, LCD VP among the 3D printing technologies useful for polymer processing.

The research was turned towards combining this material-efficient printing process with environmentally friendly materials, such as the bio-based acrylate epoxidized soybean oil (AESO) resin filled with a commercial lignin. This choice was made to fill the gap in the literature on 3D printing via LCD of these materials and to highlight the advantages of its use.

As already reported in a previous paper, LCD shows many advantages with respect to the DLP 3D printing machine,[19] such as a bottom-up configuration, where the print platform is completely immersed in the vat containing the liquid resin. The light able to initiate and promote the photopolymerization reaction is given by a light-emitting diode (LED) lamp obtained by an LCD. Moreover, an LCD assures a greener printing approach, considering the lower consumption of photocurable resin and the higher printing resolution of the final components, compared with the other VP technologies.[19] Of course, particular attention should be given to the viscosity of the resin if a VP printing is combined with biodegradable AESO-based resin to realize the final composites. As is well known, polymer viscosity is a critical parameter for an LCD printing process because it must ensure an appropriate resin flowability within the vat, affect the resin recoating between consecutive layers, and control the whole photocuring process.[11,19,32] For this reason, tetrahydrofurfuryl acrylate (THFA) was added as a bio-based reactive diluent to the resin to reduce its high viscosity, not compatible with the requirements for a 3D printing process via LCD, and to improve its flowability, favouring the formation layer by layer of the final object.[19] In addition, the presence of lignin can hold significant potential in VP 3D printing due to its sustainability and biocompatibility.

MATERIALS AND METHODS

Materials

Photocurable formulations were prepared using an AESO resin as polymer matrix. It is a viscous yellow liquid with CAS 91722-14-4, purchased from Merck (Darmstadt, Germany, with a density of 1.04 g/cm^3 at 25 °C. The chemical structure and Fourier transform IR (FTIR) spectrum of the pristine AESO resin are reported in Figs S1 and S2 of the Supplementary Information.

THFA was used as reactive diluent and phenyl bis(2, 4,6-trimethylbenzoyl) phosphine oxide (BAPO) as photoinitiator, all purchased from Merck (Darmstadt, Germany). UPM BioPiva™ 395 was the kraft softwood lignin used as natural filler, purchased from UPM Biochemicals (Helsinki, Finland).

Photocurable formulations

Unfilled AESO-based formulations were prepared by mixing the resin with THFA (60:40 wt/wt), in the presence of 2 wt% BAPO as initiator for free radical photopolymerization. Bio-based composites were prepared by adding lignin up to 10 parts per hundred

Polymer International published by John Wiley & Sons Ltd on behalf of Society of Chemical Industry.

resin (phr) to the AESO-THFA formulation. The lignin-based samples are coded AESO-THFA + L5, AESO-THFA + L7.5 and AESO-THFA + L10, respectively. The brown lignin powder was dispersed within the photocurable polymer matrix by alternating 30 min of magnetic stirring and 30 min of ultrasonic bath for a total of 3 h.

3D printing of lignin-based samples

The AESO-based formulations were printed by employing an LCD Phrozen Sonic Mini 8 K VP 3D printer, equipped with a 50 W linear projection LED module as its light source, which operates at a UV wavelength of 405 nm, and a printing volume of 16.5 cm length, 7.2 cm width and 18.0 cm height. The Chitubox software provides several options for selecting the orientation of the part into the printing volume, applying supports that connect the piece to the printing platform and adjusting the printing parameters, such as exposure time, layer thickness and platform velocity. Once the printability of each formulation was studied and the printing parameters were set, the 3D printed samples were removed from the platform, washed with 1-butanol to remove traces of unreacted monomers or photoinitiator, and post-cured for 30 min through an Anycubic Wash and Cure Plus system equipped with a UV lamp operating at a wavelength of 405 nm with a maximum power output of 40 W. The machine measures 290 mm in length, 270 mm in width and 479 mm in height.

Characterization

The morphology of the lignin powder and 3D printed samples was investigated using a Phenom™ XL scanning electron microscope (Massachusetts, USA) at a voltage of 15 kV. Each specimen was previously fractured in liquid nitrogen and the fracture surfaces were analysed after metallization with platinum.

Granulometric analysis of lignin powder was performed by using an automated particle size and shape analyser Morphology 4 (Malvern Panalytical, UK). The tests were carried out on a volume of 3 mm^3 of dry powder dispersed onto a glass plate, with an injection time of 10 ms and a high-pressure dispersion of 4 bar.

TGA was carried out on the lignin powder and the 3D printed samples using a METTLER TOLEDO TGA 851e instrument (Columbus, OH, USA), from 25 to 900 °C with a heating rate of 10 °C min^{-1} and 50 mL min^{-1} of air flow.

The viscosity of the liquid photocurable AESO-based formulations was evaluated at room temperature employing an MCR 702e multidrive rheometer (Anton Paar, Graz, Austria) in a parallel plate configuration, with a plate diameter of 25 mm. Measurements were carried out across a frequency range from 0.1 to 1000 Hz, and the output dynamic viscosity was recorded in Pascal seconds. The measuring gap was set to 0.200 mm.

FTIR spectroscopy was used to study the acrylate group conversion by means of a Nicolet iS 50 FTIR spectrometer (Thermo Fisher Scientific, Waltham, MA, USA), with spectra acquired before and after curing through 32 scans at a spectral resolution of 4 cm^{-1}. Data were recorded and analysed with Omnic software. A Hamamatsu LIGHTINGCURE LC8 mercury lamp (Hamamatsu Photonics) with fibre-optic delivery was employed, emitting UV light centred at 365 nm and with an intensity of 580 mW cm^{-2}.

The photocuring process was tracked by observing the reduction in peak intensity at 810 cm^{-1}, characteristic of the acrylate groups. The conversion was calculated monitoring the decrease in the area of the absorption band of the reactive acrylate functionality as a function of the irradiation time. The area was normalized by a constant signal in the spectra, the ester C=O stretching peak at 1730 cm^{-1} serving as an internal reference. The kinetic conversion was given following the equation reported in the literature.[33,34]

The gel content of the photocured specimens was measured according to the specifications of the ASTM D2765-84 standard, after 24 h of extraction with chloroform.

The dynamic mechanical thermal analysis (DMTA) tests were performed, using an Anton Paar MCR 702e multidrive device (Graz, Austria), by applying uniaxial sinusoidal stress with an amplitude of 1 N and a frequency of 1 Hz on rectangular samples with dimensions of 35 mm length, 10 mm width and 2 mm thickness.

The tensile properties of 3D printed samples (type 5A) were also tested on dogbone-shaped specimens by using tensile tests according to ISO 527-2 standard, using an Instron 5966 with a 2 kN load cell and pneumatic grips, with a grip separation of 50 mm and a deformation rate of 2 mm min^{-1}. The deformation was determined using a displacement transducer. Each specimen featured a gauge length of 26 mm, a width of 4 mm and a thickness of 3 mm.

Water contact angle measurements of the 3D printed samples unfilled and filled with lignin were performed using a contact angle analysis equipment OCA20 Data Physics. A drop of 10 µL of distilled water was syringed onto the sample surface, using an electronic syringe Hamilton DS500/GT with a dosing rate of 5 µL s^{-1}. The image of the drop was immediately captured and analysed to yield a contact angle value. Five different measurements were carried out on different areas for each sample and the average value is reported.

RESULTS AND DISCUSSION

Lignin characterization

The morphology of pristine lignin was investigated by SEM analysis to evaluate its particle shape and dimensions. Figure 1 presents SEM images of lignin at different magnifications, 500× and 2000×. As can be seen, lignin powder is characterized by irregular particles of size less than 100 µm, which tend easily to form aggregates. The SEM micrographs indicate that the lignin has submicron particles which can form aggregates in the dry state.

The granulometric analysis performed by acquiring images of thousands of lignin particles led to a representation of the morphological features of the lignin powder, in terms of particle size distribution and diameter (Fig. 1(c)). The lignin particles were found to have a particle size distribution with an average diameter of 4.5 µm.

TGA and derivative thermogravimetry (DTG) analyses were also performed to study the lignin thermal behaviour. The thermograms of Fig. 2 present the TGA and DTG curves of lignin performed in air from room temperature to 900 °C.

Lignin is moderately stable at high temperatures (up to 200 °C) due to its characteristic aromatic backbone.[32] As is visible from Fig. 2, lignin degradation involves two main stages with a major weight loss between 300 and 500 °C. The first degradation peak is located at 262 °C, due to the elimination of formic acid, formaldehyde, carbon dioxide, sulfur dioxide and water, as already reported in the literature.[32] A second degradation step corresponding to a peak temperature of 466 °C can be attributed to the presence of remaining carbohydrates in lignin, such as hemicellulose.[32]

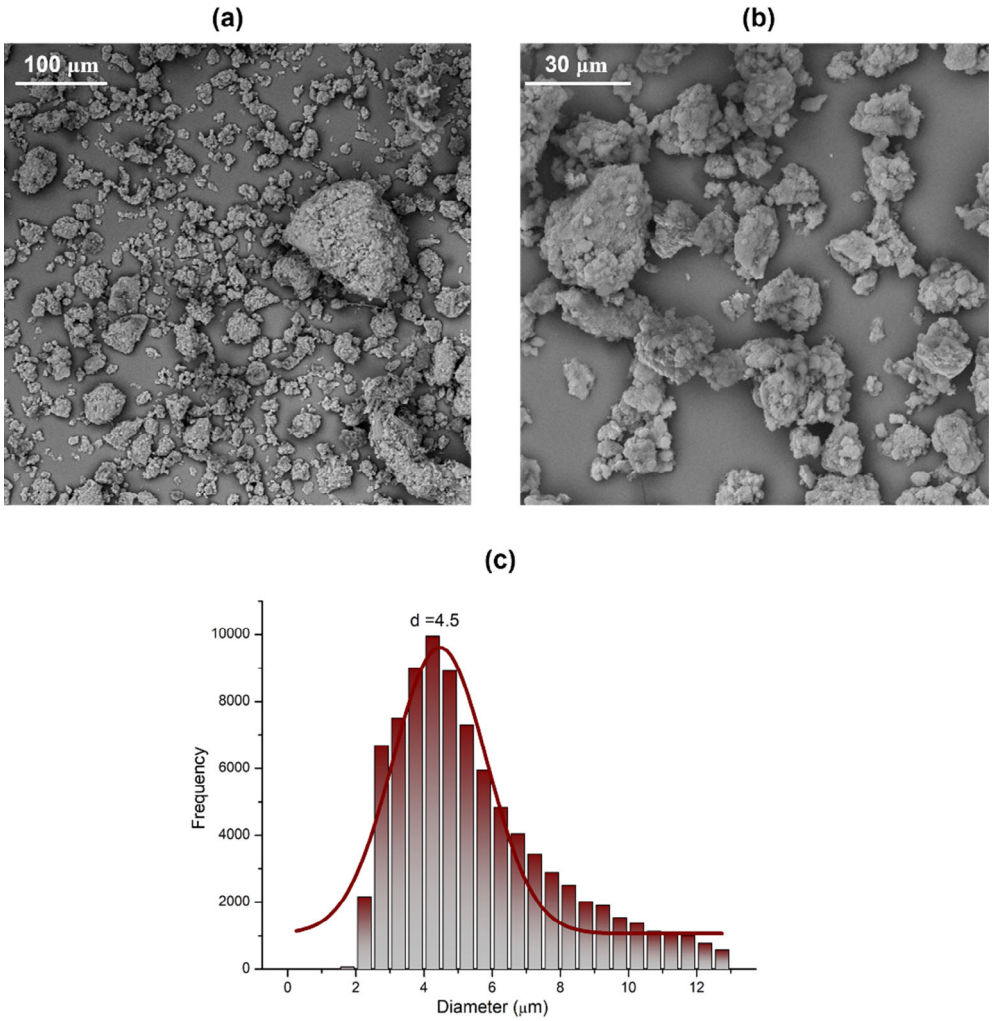

Figure 1. SEM micrographs at different magnifications (a), (b) and particle size distribution (c) of lignin.

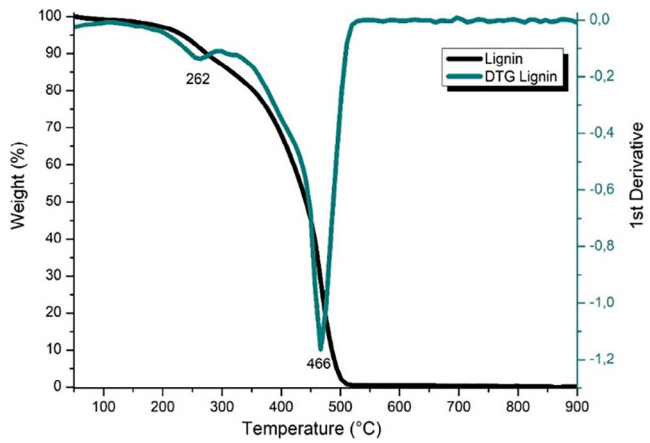

Figure 2. TGA and DTG curves of lignin powder performed in air.

Preparation of AESO-based formulations

Samples containing 60 wt% AESO and 40 wt% THFA were prepared via LCD and used as a reference system. Lignin particles were mixed within the photocurable formulations at different concentrations, starting from 5 up to 10 phr.

After the formulation's preparation, several sedimentation tests were conducted to evaluate whether the mixtures can maintain their characteristics over time by analysing the stability of the dispersed lignin particles, which can be comparable with the time within the printer. If the filler tends to sediment or separate quickly, it indicates a low dispersion stability which can lead to printing defects, as the filler is not uniformly distributed within the photocurable liquid resin. The sedimentation tests, performed for each formulation containing lignin, allow a continuous monitoring of the mixture's behaviour over time in the interval from 1 h up to 24 h, and let the ideal geometries to print be chosen, which are strictly dependent on the printing time and the amount of filler. Due to the brown colour of lignin, the formulations appear too dark to give an indication of the filler dispersion within the AESO-THFA resin after 8 h. For this reason, only geometries requiring a level of complexity within the interval of the filler sedimentation were effectively selected for the printing process.

Then, the zero-shear viscosity was evaluated to study the effect of the lignin addition on the resin flowability, considering that the dispersion of a filler within a polymeric matrix is expected to increase the viscosity of the liquid resin and thus can significantly affect its printability via VP.[19,31] Resin viscosity can be identified as the most important parameter for compatibility with an LCD printing process due to its tendency to affect the resin recoating

Table 1. The viscosity of AESO-based formulations filled with different amounts of lignin

Sample code	Viscosity at 25 °C and 1 Hz (Pa s)
AESO-THFA	0.7
AESO-THFA + L5	2.5
AESO-THFA + L7.5	5.8
AESO-THFA + L10	15.8

procedure over the surface between two successive layers. In fact, high viscosity values result in longer print times and lower scan speeds.[19] To deal with the viscosity problem, the relatively high AESO viscosity was reduced by the addition of THFA as reactive diluent. The viscosity measurements of the unfilled and filled AESO-THFA formulations, evaluated at 25 °C and a frequency of 1 Hz, are reported in Table 1.

As expected, the viscosity strongly increases on increasing the lignin content, which implies a limit to the amount of lignin that the AESO-THFA resin can host whilst remaining in an acceptable viscosity range for 3D printing.[19] All the samples show a shear-thinning behaviour at low frequencies, while on increasing the frequency their behaviour becomes pseudo-Newtonian and therefore the viscosity remains constant. Moreover, the addition of lignin up to 10 phr led to a drastic increase in the viscosity of the suspension, reaching values that exceed the range recommended for the VP process. These findings allow one to imagine a critical scenario for the printing process of lignin-based composites filled with a high amount of lignin. In fact, high values of viscosity can negatively influence the curing process and the resin flowability within the printer, thereby altering the final composite properties and performance.[35–37] Anyway, the formulation with 10 phr lignin was also used for the subsequent study of printability.

3D printing process via LCD

Different tests were first performed to set the effective printing parameters and to investigate the printability of the prepared formulation via LCD. The optimization of the printing parameters was done by means of a comprehensive experimental testing procedure for each photocurable formulation. Initially, the printability of the AESO-based formulations was assessed, starting from printing parameters reported in previous literature on similar resins.[19] Then, a systematic optimization of the relevant settings for the preparation of the composite formulations was carried out. The optimized parameters for the preparation of the AESO-based samples are reported in detail in Table 2.

The exposure time significantly increases in the presence of lignin and on increasing the amount of lignin particles, while the curing rate decreases. This is because lignin contains several UV-active moieties in its structure, such as aromatic rings and C=O bonds, which can absorb UV photons and act as UV blockers.[32] Consequently, this can retard the penetration of UV light given by the LCD screen, increasing the time of curing, strongly decreasing the curing rate and negatively influencing the viscosity of the resin and the dispersion of lignin within the photocurable formulation, which can precipitate and form aggregates in the presence of a high amount of lignin particles (10 phr). Considering all these factors, different kinds of samples were successfully 3D printed starting from simple geometries up to more challenging architectures.

Figure 3 reports some examples of 3D printed parts containing 60 wt% AESO and 40 wt% THFA, unfilled and filled with different amounts of lignin and realized via LCD. The figures represent typical cube-shaped lattice structures realized with different numbers of layers (200 and 400) and, in the case of the unfilled resin, an octahedron made of 100 layers with a singular internal pattern characterized by full and empty spaces and thin circular holes. The unfilled AESO-THFA samples (Fig. 3(a)) have high resolution, dimensional accuracy and a good level of detail. The images show high-density cube-shaped lattice designs and hollow honeycomb-like cells. A visual evaluation of the printed parts reveals that also the lignin-based composite samples have a high resolution and accuracy, good layer adhesion and edge definition without significant defects (Figs 3(b)–3(d)).

The 3D objects obtained by adding lignin to the polymeric matrix display a significant change of colour due to the presence of the filler, which acts as a natural colourant giving a brown colour to the final specimens.

Moreover, Fig. 3(e) shows dogbone and rectangular specimens obtained by dispersing lignin at 10 phr. In fact, because of the high viscosity and low flowability of the formulation within

Table 2. LCD printing parameters for AESO-based resins and composites

Parameter	AESO-THFA	AESO-THFA + L5	AESO-THFA + L7.5	AESO-THFA + L10
Layer height (mm)	0.1	0.1	0.1	0.1
Exposure time (s)	18	25	28	30
Bottom exposure time (s)	40	360	400	450
Rest time before lift (s)	0	4	4	4
Rest time after lift (s)	5	1	1	1
Rest time after retract (s)	3	4	4	4
Bottom lift distance (mm)	6	8	8	8
Lifting distance (mm)	6	8	8	8
Bottom retract distance (mm)	6	8	8	8
Retract distance (mm)	6	8	8	8
Bottom lift speed (mm min^{-1})	90	70	70	70
Lifting speed (mm min^{-1})	90	70	70	70
Bottom retract speed (mm min^{-1})	170	150	150	150
Retract speed (mm min^{-1})	170	150	150	150

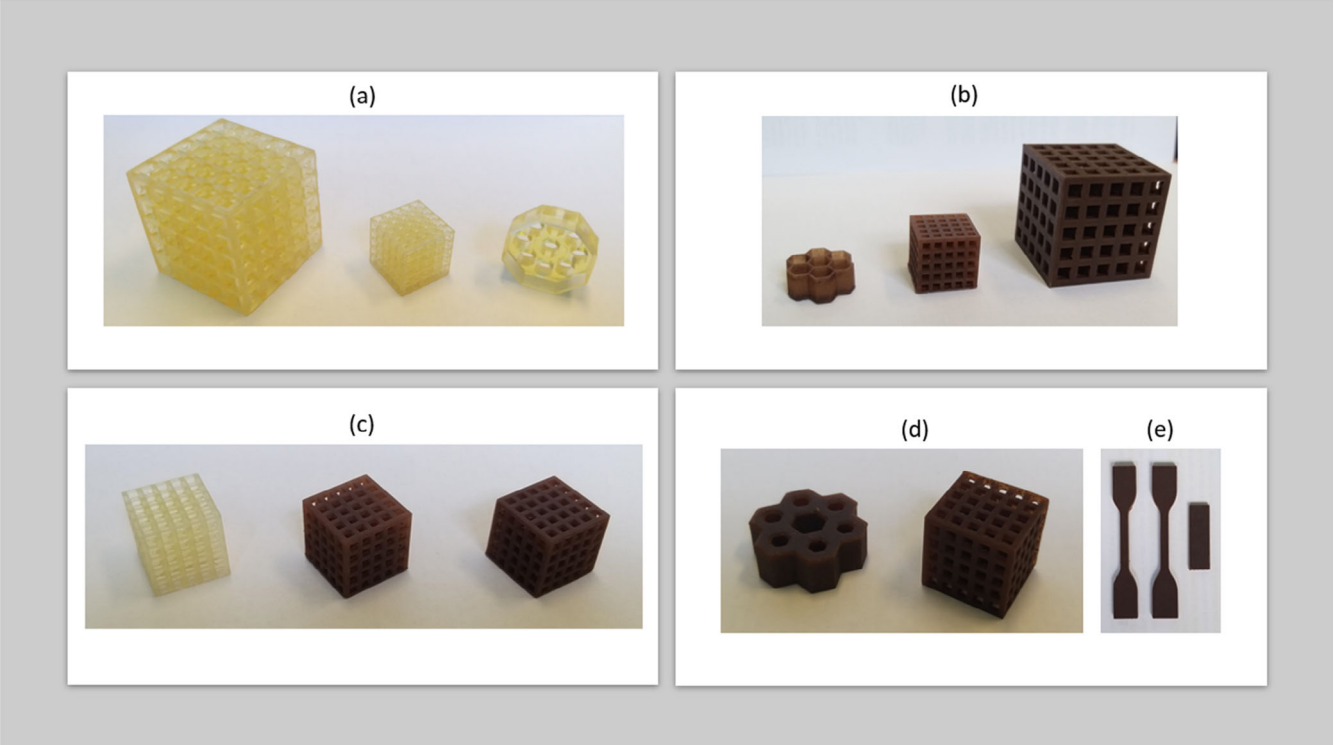

Figure 3. 3D printed samples containing 60 wt% AESO and 40 wt% THFA unfilled (a), and filled with different amounts of lignin: 5 phr (b), 5 and 7.5 phr (c), 7.5 phr (d) and 10 phr (e).

the vat, it was not possible to print more complex geometries. This can be attributed to the tendency of the brown lignin particles to hinder the photocuring process during the printing leading to an increase of the curing time and the viscosity of the resin, and consequently influencing its printability within the LCD printer.[32]

FTIR spectroscopy

The acrylate group conversion occurring during the photocuring process was investigated by FTIR spectroscopy by analysing the reduction in peak intensity relative to the acrylate group located at 810 cm^{-1} using as a reference the C=O ester stretching peak at 1730 cm^{-1}. This spectroscopic technique enables *in situ* monitoring of chemical processes by tracking the disappearance of characteristic bands associated with the reactive monomer during UV exposure.

Figure 4(a) illustrates the FTIR spectra of the acrylate groups monitored as a function of irradiation time from zero to 120 s for the unfilled AESO-THFA. To evaluate the effect of the presence of lignin on the UV-curing process, FTIR analyses were also performed on the AESO-based photocurable formulations containing increasing content of lignin: AESO-THFA + L5, L7.5 and L10, reported in Figs 4(b)–4(d).

The peak of the acrylates in the neat photocurable formulation and in the filled ones shows a strong decrease after a few seconds of UV irradiation revealing that the photocuring reaction is fast enough to allow complete conversion of the acrylate's functionalities after 120 s. No shift or significant change in peak shape was observed in the composite sample spectra which appear almost superimposed.

To examine the reaction progression as a function of the irradiation time, a kinetic FTIR spectroscopy analysis was conducted on the unfilled acrylate system (AESO-THFA) as well as on the lignin-loaded acrylate systems AESO-THFA + L5, L7.5 and L10. Figure 5 presents the percentage conversion of the acrylate reactive group for all the AESO-based photocurable formulations, which starts at 0% for all the systems at time zero and increases rapidly in the first 10 s, followed by a slower rise towards a plateau.

The qualitative trends are consistent: AESO-THFA and AESO-THFA + L5 show the highest overall conversion, which reaches percentage values of 96% and 95%, followed by the systems filled with an increasing amount of lignin up to 10 wt%, which slightly underperforms the others, as is visible from the data of Table 3. This behaviour suggests an optimal additive concentration close to 5 wt%, with diminishing benefits or potential inhibition at higher levels. Increasing the lignin content within the AESO-based system results in a reduction in the degree of acrylate conversion up to 93%. This effect can probably be attributed to the brown colouration of lignin, which can absorb the incident UV radiation, negatively affecting the photocuring process.

Insoluble fraction

The conversion of the acrylate reactive groups seen before has been further confirmed by the high gel content values obtained for the photocured specimens.

All the AESO-based samples showed gel content values higher than 99% after the extraction in chloroform. The results indicate that the addition of lignin within the AESO-THFA matrix does not have an effect on the photocured polymer network formation, as is clear from the data reported in Table 3. This emphasizes that the selected printing parameters are useful for achieving high values of monomer conversion during the photocuring process occurring within the 3D printer.

Morphology of lignin-based composites

The morphology of the photocured materials, unfilled and filled with lignin and realized via LCD, was examined by means of

Polymer International published by John Wiley & Sons Ltd on behalf of Society of Chemical Industry.

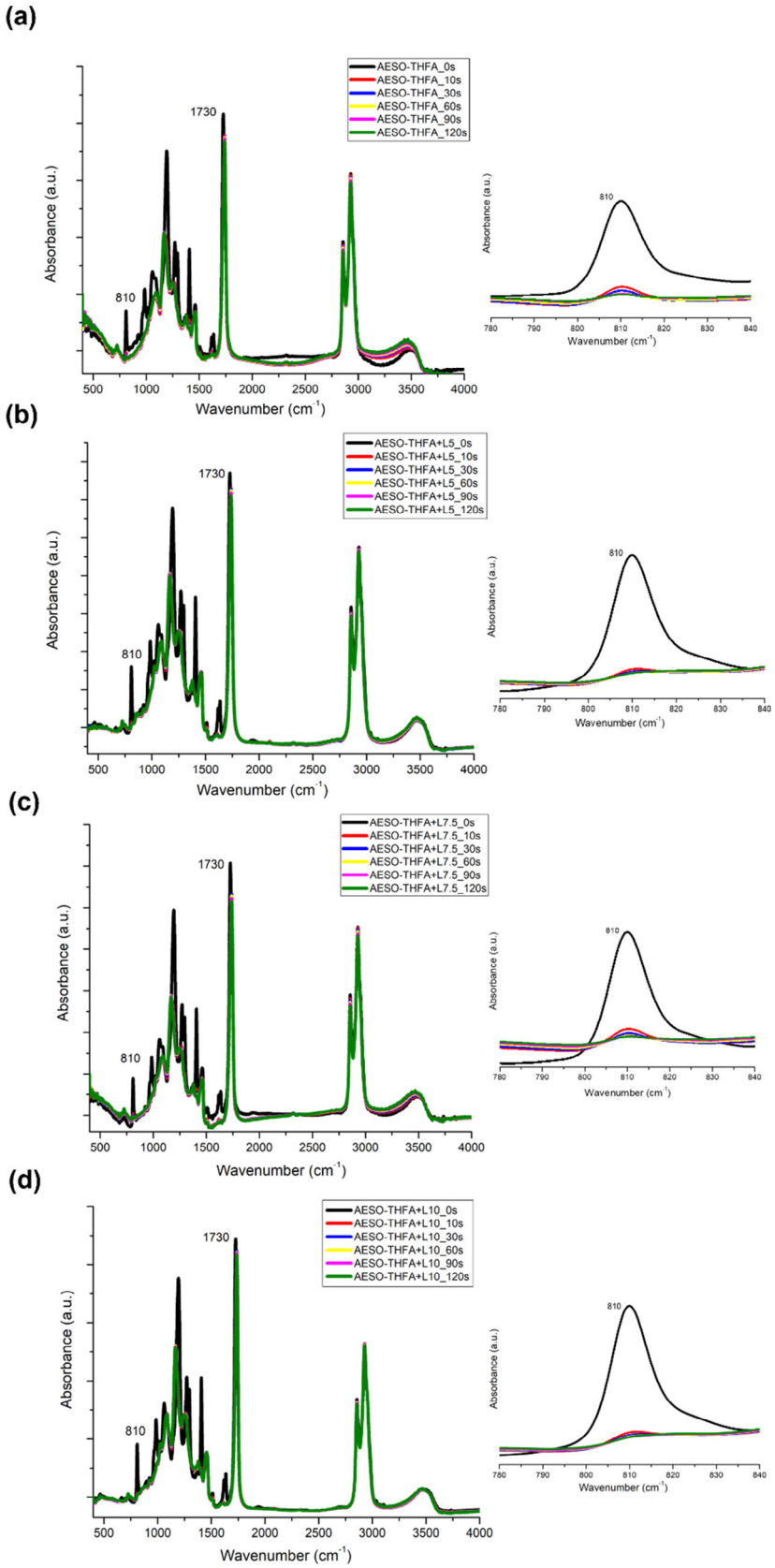

Figure 4. FTIR spectra of the acrylate functional groups of AESO-THFA photocurable formulations unfilled (a) and filled with lignin: L5 (b), L7.5 (c) and L10 (d). An enlargement of the spectrum range related to the C=O acrylate groups is also reported for all the systems investigated.

Polymer International published by John Wiley & Sons Ltd on behalf of Society of Chemical Industry.

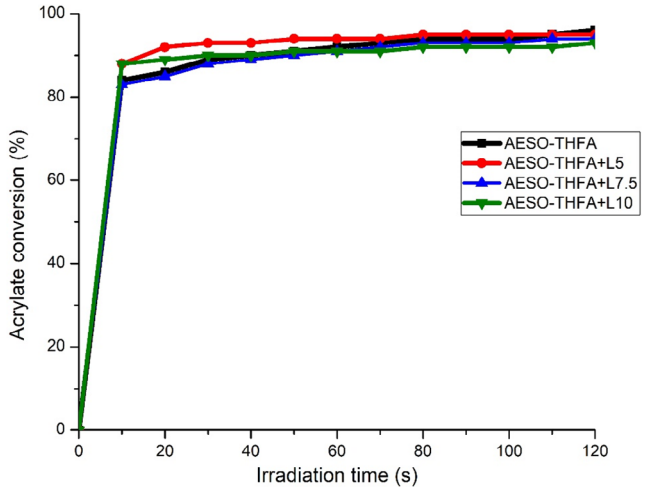

Figure 5. Conversion comparison as a function of the irradiation time for the unfilled AESO-THFA formulation (black line) and for the formulations filled with lignin: L5 (red line), L7.5 (blue line) and L10 (green line).

SEM micrographs, at 500× magnification. The fracture surface of the unfilled system appears smooth and homogeneous since no filler has been incorporated (Fig. 6(a)). The lignin-based composites examined show a good distribution of the lignin within the cured resin for the samples containing 5 and 7.5 phr filler, as evidenced by the SEM micrographs of Figs 6(b) and 6(c), respectively.

In contrast, some agglomerates are evident on increasing the filler content to 10 phr due to the tendency of the lignin particles to aggregate during the printing process after a long time, as reported in Fig. 6(d), where the filler appears to be clustered around the fracture surfaces of the specimen. This result can surely be attributed to the higher printing times and lower speeds occurring during the printing process in the presence of 10 phr lignin, because the filler particles act as UV absorbers and significantly slow down the curing process.[38,39]

Thermal and thermomechanical properties of lignin-based composites

The thermal properties of the lignin-based 3D printed samples were studied using TGA. Figure 7 presents the TGA and DTG curves of the samples obtained by mixing THFA as the reactive diluent and the composites filled with different concentrations of lignin: 5, 7.5 and 10 phr. The thermograms of Fig. 7(a) show the same thermal behaviour for all the tested samples to underline that the addition of lignin to the AESO-THFA matrix and the printing process do not affect the final thermal stability of the matrix in a significant way.[25] As is visible from the data of Table 2, the onset degradation temperatures at which there is a 5 wt% weight loss (T_5) slightly shift toward lower temperatures in the presence of lignin. The temperatures at which there is a 50 wt% weight loss (T_{50}) show almost the same values.

The thermal degradation for all the printed samples involves two main steps, as can be seen in the DTG curves reported in Fig. 7(b). The first degradation step occurs at 387 °C for the unfilled system and at around 380 °C for the composites filled with lignin. The same behaviour can be seen for the second degradation stage, which occurs at 557 °C for the pristine AESO-THFA sample and shifts toward lower temperatures for the lignin-based composites (532 °C) for samples with 10 phr of lignin. This can be explained by considering that the presence of a higher amount of lignin hinders the curing process during printing and leads to a slight reduction in the degradation and thermal stability of the lignin-based composites.[36–39]

DMTA was also performed to evaluate the tan δ curves of the unfilled and lignin-based systems, as reported in Fig. 8.

The temperature at which the transition from a glassy state to a rubbery one occurs for a thermosetting resin, marked by the maximum of the tan δ curves as a function of temperature, corresponds to the glass transition temperatures. It can be seen from the tan δ curves of Fig. 8 that the glass transition values slightly decrease on increasing the lignin content, from 15 to 10 °C. This result suggests that the tested lignin-based specimens move from the glassy state to the rubbery state as more lignin is incorporated within the AESO formulation.

Mechanical properties of lignin-based composites

The mechanical properties of the photocured lignin-based samples were also examined by tensile tests evaluating elastic modulus, tensile strength and elongation at break percentage. The data results and their standard deviations are summarized in Table 4. The tensile tests indicate that the addition of lignin led to a slight decrease of the elastic modulus and the ultimate tensile strength of the composites. The elastic modulus shifts from 15 MPa for the unfilled system to 13.5 MPa for the composites loaded with the highest lignin content. At the same time, the tensile strength

Table 3. Acrylate conversion degrees, gel contents, thermal properties and water contact angles of lignin-based samples

Sample code	Acrylate conversion (%)	Gel (%)	T_5[a] (°C)	T_{50}[b] (°C)	$T_{max\ deg}$[c] (°C)	Residue[d] (%)	T_g[e] (°C)	Water contact angle (°)
Lignin	–	–	237	440	262/466	0	–	–
AESO-THFA	96	99.2	317	392	387/557	0.5	15	85 ± 4
AESO-THFA + L5	95	99.5	315	391	380/532	0.6	13	90 ± 4
AESO-THFA + L7.5	94	99.2	308	390	381/533	0.8	11	86 ± 4
AESO-THFA + L10	93	99.3	290	390	381/532	1.2	10	86 ± 3

[a] Temperature at which there is 5 wt% weight loss.
[b] Temperature at which there is 50 wt% weight loss.
[c] Maximum degradation peak temperature determined by DTG curves.
[d] Residue determined by TGA at 900 °C.
[e] T_g determined by DMTA.

Polymer International published by John Wiley & Sons Ltd on behalf of Society of Chemical Industry.

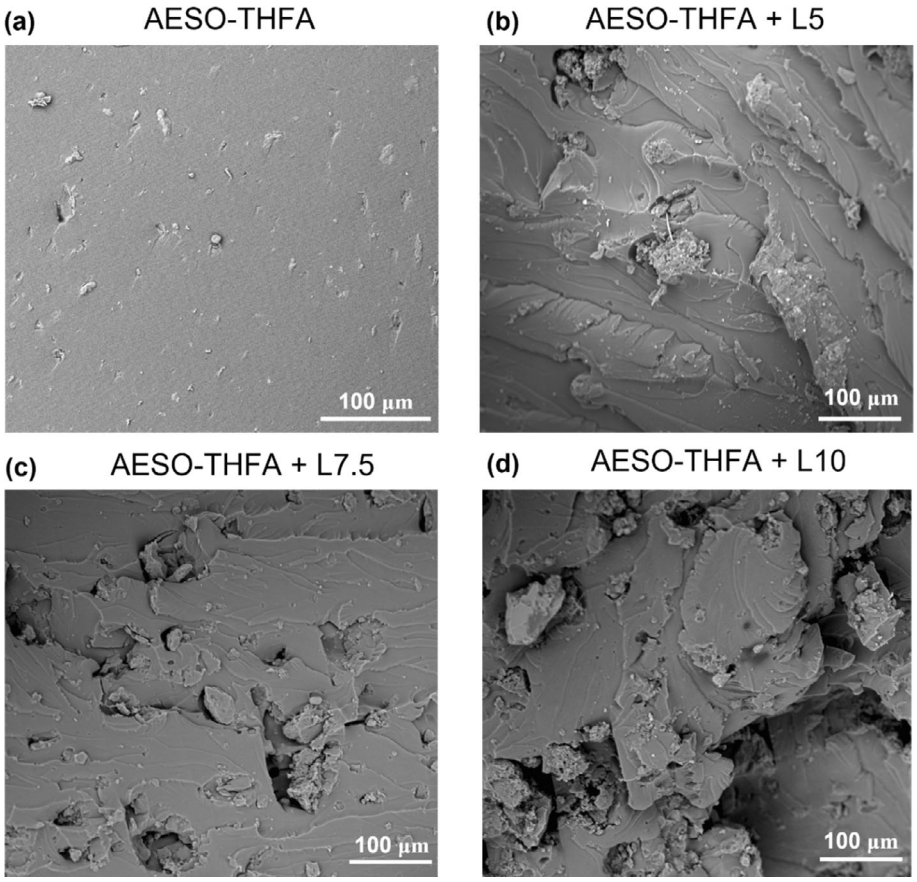

Figure 6. SEM micrographs of the fracture surface of a 3D printed AESO-THFA sample (a) and specimens filled with lignin: L5 (b), L7.5 (c) and L10 (d).

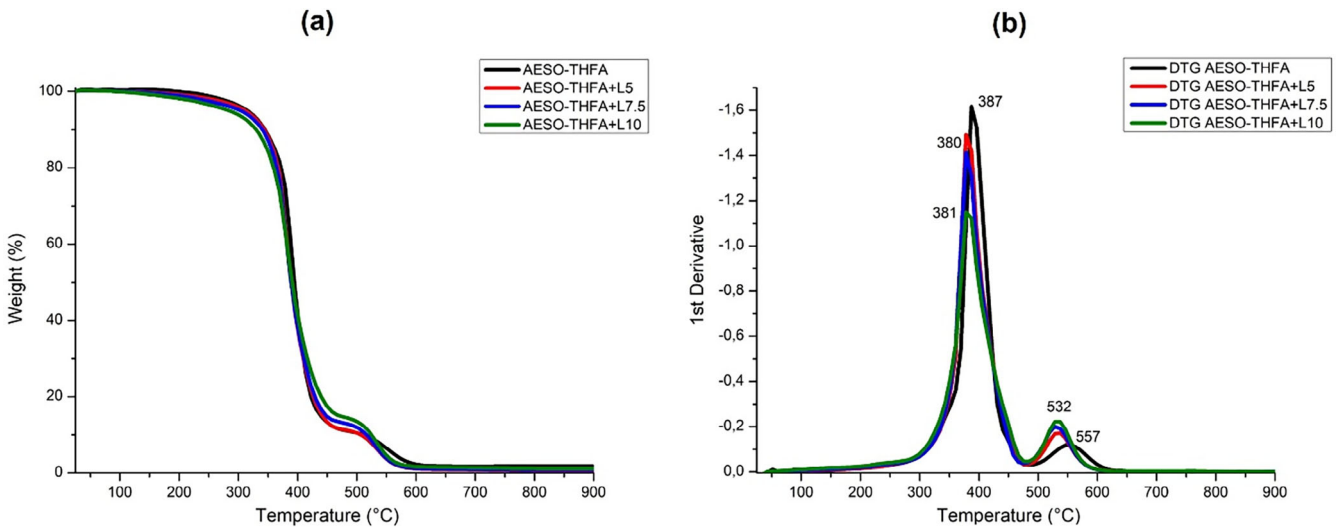

Figure 7. TGA and DTG curves of 3D printed samples unfilled or filled with lignin.

slightly decreases in the presence of lignin from 3 MPa for the unfilled system to 1.1 MPa for composites containing a higher amount of filler particles (10 phr).

The decrease in the tensile properties of the lignin-based composites can be attributed to the lignin particles not homogeneously dispersed within the polymeric matrix, as already seen from SEM micrographs, which negatively affects the final mechanical properties of the composites. Moreover, it is possible to see a slight increase in the flexibility of the polymeric systems because the lignin particles can also act as plasticizers, as already reported in the literature.[32,38]

When incorporated into a cured resin, the lignin can interact with the polymer network reducing the crosslinking density and the rigidity of the system. Therefore, it can enhance the chain

Polymer International published by John Wiley & Sons Ltd on behalf of Society of Chemical Industry.

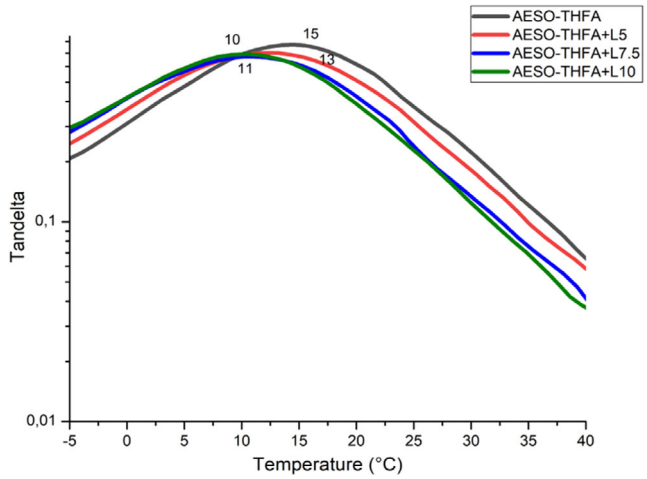

Figure 8. Tan δ curves of 3D printed samples unfilled or filled with lignin.

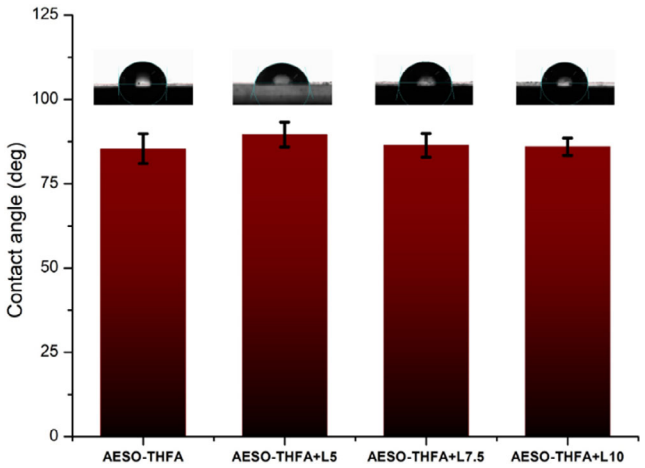

Figure 9. Water contact angles of 3D printed samples unfilled or filled with lignin.

mobility and make the final resin more flexible.[32,36] Moreover, the presence of lignin can lead to a reduction of the glass transition temperatures, as already seen in the DMTA results. Further studies need to be done to increase the lignin dispersion within the polymeric resin to have a better mechanical response and to make these kinds of composites more competitive for 3D printing applications with respect to traditional ones.

Wettability of lignin-based composites

Lignin is characterized by a complex structure and thus can have either a hydrophobic or hydrophilic behaviour.[40,41] Specifically, kraft lignin shows a high hydrophobic character due to the presence of sulfur atoms introduced into its structure by the kraft modification reaction.[41,42] For this reason, contact angle measurements with water were performed to determine the surface wettability of the AESO-THFA photocured samples induced by the addition of lignin. It is worth noting that the presence of lignin within the crosslinked network leads to a slight decrease of the water contact angles values, as illustrated in Fig. 9.

The lignin-based composites containing 5 phr lignin show an increase of hydrophilicity probably due to the uniform dispersion of lignin particles within the AESO-THFA matrix, indicating a possible application prospect in food packaging.[43] The water contact angles for the composites prepared by increasing the lignin content remain almost the same, probably because of the presence of aggregates of particles, as previously seen by SEM analysis.

CONCLUSION

Introducing lignin to the 3D printing research field, it is possible to design and develop more sustainable polymeric composites highlighting its challenges and opportunities. Different amounts of lignin up to 10 phr were added to an AESO-based resin in the presence of THFA as reactive diluent to decrease the resin viscosity and BAPO as photoinitiator to promote the radical photopolymerization reaction.

Once the printing parameters were optimized, different models were realized, via LCD as the VP process and by adding lignin to the AESO-THFA formulation. The printed objects vary from simple rectangular and dogbone to cube-shaped lattice, octagon and honeycomb-like cell structures up to 400 layers.

The research proposes an alternative route to bring the full potential of lignin-based composites for many applications fields, using 3D printing as a greener alternative for thermoset processing. The results reveal that lignin is well dispersed within the photocured resin up to 7.5 phr. Some agglomerates are evident for samples containing higher lignin content, such as 10 phr, as revealed by SEM analysis. This can be due to the higher printing times induced to the UV blocker effect caused by the dark brown lignin particles.

The presence of lignin also led to a slight increase of the glass transition temperature values as determined by DMTA, whereas the thermal stability remains the same, as evaluated by TGA. From a mechanical point of view, an increase of flexibility was observed in the presence of lignin. Moreover, lignin dispersed within the crosslinked AESO-based polymeric network leads to a slight decrease of the water contact angles because of the hydrophilicity introduced by the lignin particles into the polymeric system.

This study can open the way to increasing the opportunity to develop fully bio-based composites by using lignin to promote the development of greener and more sustainable materials and engineered products. The ongoing research is paving the way for its broader application in realizing eco-friendly and high-performance 3D printed products in many application fields.

Improvements in lignin-based polymeric materials remain necessary to solve the problem of the filler dispersion within the

Table 4. Tensile properties of lignin-based samples

Sample code	Young's modulus (MPa)	Tensile strength (MPa)	Elongation at break (%)
AESO-THFA	15.0 ± 1.0	3.0 ± 1.0	22 ± 9.0
AESO-THFA + L5	12.0 ± 0.4	0.7 ± 0.2	6.2 ± 1.3
AESO-THFA + L7.5	13.0 ± 0.5	0.9 ± 0.1	7.1 ± 0.8
AESO-THFA + L10	13.5 ± 0.5	1.1 ± 0.1	9.7 ± 0.5

polymeric resin to add higher amounts of lignin, optimization of the printing parameters to expand the design flexibility by printing more complex architectures, and enhancement of the mechanical performance of the final objects.

ACKNOWLEDGEMENTS

The authors thank Gianluigi Chianese for his support. Open access publishing facilitated by Politecnico di Torino, as part of the Wiley - CRUI-CARE agreement.

FUNDING INFORMATION

The present work was financed by European Union MICS (made in Italy—Circular and Sustainable) Extended Partnership and the European Union Next-Generation EU (Piano Nazionale Di Ripresa E Resilienza (PNRR)—Missione 4 Componente 2, Investimento 1.3—D.D. 1551.11-10-2022, PE00000004). The manuscript reports the authors' viewpoints; neither the European Union nor the European Commission can be responsible for them.

CONFLICT OF INTEREST

All the authors declare no known conflict of interest.

SUPPORTING INFORMATION

Supporting information may be found in the online version of this article.

REFERENCES

1 Alghamdi SS, John S, Roy Choudhury N and Dutta NK, *Polymers* **13**: 753–791 (2021). https://doi.org/10.3390/polym13050753.
2 Jandyal A, Chaturvedi I, Wazir I, Raina A and Haq MIU, *Sustainable Operations and Computers* **3**:33–42 (2022). https://doi.org/10.1016/j.susoc.2021.09.004.
3 Jasiuk I, Abueidda DW, Kozuch C, Pang S, Su FY and Mckittrick J, *JOM* **70**:275–283 (2018). https://doi.org/10.1007/s11837-017-2730-y.
4 Singha S, Ramakrishna S and Singh R, *J Manuf Process* **25**:185–200 (2017).
5 Yadav A, Rohru P and Babbar A, *Int J Interact Des Manuf* **17**:2867–2889 (2023). https://doi.org/10.1007/s12008-022-01026-5.
6 Colucci G, Piano M, Lupone F, Badini C, Bondioli F and Messori M, *Materials Today Chemistry* **33**:101687 (2023). https://doi.org/10.1016/j.mtchem.2023.101687.
7 Chaudhary R, Fabbri P, Leoni E, Mazzanti F, Akbari R and Antonini C, *Progress in Additive Manufacturing* **8**:331–351 (2023). https://doi.org/10.1007/s40964-022-00336-0.
8 Ligon SC, Liska R, Stampfl J, Gurr M and Mülhaupt R, *Chem Rev* **117**: 10212–10290 (2017).
9 Medellin A, Du W, Miao G, Zou J, Pei Z and Ma C, *J Micro Nano-Manuf* **7**: 31006–31017 (2019). https://doi.org/10.1115/1.4044288.
10 Chen J, Liu H, Lv L and Liu Z, *J Appl Polym Sci* **137**:48827 (2020). https://doi.org/10.1002/APP.48827.
11 Noé C, Cosola A, Tonda-Turo C, Sesana R, Delprete C, Chiappone A *et al.*, *Polymer* **247**:124779 (2022). https://doi.org/10.1016/j.polymer.2022.124779.
12 Skliutas E, Lebedevaite M, Kasetaite S, Rekštytė S, Lileikis S, Ostrauskaite J *et al.*, *Sci Rep* **10**:9758 (2020). https://doi.org/10.1038/s41598-020-66618-1.
13 Stanzione JF, Sadler JM, La Scala JJ and Wool RP, *ACS Sustain Chem Eng* **1**:419–426 (2013). https://doi.org/10.1021/sc3001492.
14 Bassett AW, Honnig AE, Breyta CM, Dunn IC, La Scala JJ and Stanzione JF, *ACS Sustain Chem Eng* **8**:5626–5635 (2020). https://doi.org/10.1021/acssuschemeng.0c00159.
15 Navaruckiene A, Skliutas E, Kasetaite S, Rekštyte S, Raudoniene V, Bridziuviene D *et al.*, *Polymers* **12**:397 (2020). https://doi.org/10.3390/polym12020397.
16 Melilli G, Carmagnola I, Tonda-Turo C, Pirri F, Ciardelli G, Sangermano M *et al.*, *Polymers* **12**:1655 (2020). https://doi.org/10.3390/polym12081655.
17 Placone JK, Navarro J, Laslo GW, Lerman MJ, Gabard AR, Herendeen GJ *et al.*, *Ann Biomed Eng* **45**:237–248 (2017). https://doi.org/10.1007/s10439-016-1621-7.
18 Yoha KS and Moses JA, *Foods* **12**:212 (2023). https://doi.org/10.3390/foods12010212.
19 Colucci G, Sacchi F, Bondioli F and Messori M, *Polymers* **16**:1272–1287 (2024). https://doi.org/10.3390/polym16091272.
20 Arias-Ferreiro G, Lasagabáster-Latorre A, Ares-Pernas A, Ligero P, María García-Garabal S, Dopico-García MS *et al.*, *Polymers* **14**:4164 (2022). https://doi.org/10.3390/polym14194164.
21 Yoon J, Hong IS, Khang G, Lee SJ, Yoo JJ and Hum PC, *Nat Commun* **9**: 1620–1633 (2018) DOI: 10.1038/s41467-018-03759-y, 9.
22 Kumar A, Anushree A, Kumar J and Bhaskar T, *J Energy Inst* **93**:235–271 (2020). https://doi.org/10.1016/j.joei.2019.03.005.
23 Gellerstedt GLF and Henriksson EG, *Monomers Polym Compos Renew Resour* **9**:201–224 (2008). https://doi.org/10.1016/B978-0-08-045316-3.00009-0.
24 Ragauskas AJ, Beckham GT, Biddy MJ, Chandra R, Chen F, Davis MF *et al.*, *Science* **344**:1246843 (2014). https://doi.org/10.1126/science.1246843.
25 Balakshin M, Capanema EA, Sulaeva I, Schlee P, Huang Z, Feng M *et al.*, *Chem Sus Chem* **14**:1016–1036 (2021). https://doi.org/10.1002/cssc.202002553.
26 Gellerstedt G and Henriksson G, Chapter 9—Lignins: major sources, structure and properties, in *Monomers, Polymers and Composites from Renewable Resources*. Elsevier, Amsterdam (2008).
27 Brass GF and Epps T, *Polym Chem* **12**:4130–4158 (2021). https://doi.org/10.1039/d1py00694k.
28 Kadla JF and Kubo S, *Compos Part A Appl Sci Manuf* **35**:395–400 (2004). https://doi.org/10.1016/j.compositesa.2003.09.019.
29 Liu H, Mulderrig L, Hallinan D Jr and Chung H, *Macromol Rapid Commun* **42**:2000428 (2021). https://doi.org/10.1002/marc.202000428.
30 Batarseh S, Goldsberry N, Handysides C, Nemat-Bakhsh L, Valenzuela C, Caruso J *et al.*, *J Calif Dent Assoc* **51**:2271641 (2023).
31 Sen S, Patil S and Argyropoulos DS, *Green Chem* **17**:4862–4887 (2015). https://doi.org/10.1039/c5gc01066g.
32 Hatakeyama T, Yamashita S and Hatakeyama H, *J Thermal Analysis Calorimetry* **143**:203–211 (2021). https://doi.org/10.1007/s10973-019-09161-0.
33 Narewska J, Lassila L and Fardim P, *Cellul* **21**:1769–1780 (2014). https://doi.org/10.1007/s10570-013-0157-3.
34 Pezzana L, Melilli G, Guigo N, Sbirrazzuoli N and Sangermano M, *ACS Sustain Chem Eng* **9**:17403–17412 (2021). https://doi.org/10.1021/acssuschemeng.1c06939.
35 Sutton JT, Rajan K, Harper DP and Chmely SC, *ACS Appl Mater Interfaces* **10**:36456–36463 (2018). https://doi.org/10.1021/acsami.8b13031.
36 Thielemans W, Can E, Morye SS and Wool RP, *J Appl Polym Sci* **83**:323–331 (2002).
37 Ebers LS, Arya A, Bowland CC, Glasser WG, Chmely SC, Naskar AK *et al.*, *Biopolymers* **112**:e23431 (2021). https://doi.org/10.1002/bip.23431.
38 Wan Z, Zhang H, Niu M, Guo Y and Li H, *Int J Biol Macromol* **253**: 126660–126673 (2023).
39 Keck S, Liske O, Seidler K, Steyrer B, Gorsche C, Knaus S *et al.*, *Biomacromolecules* **24**:1751–1762 (2023). https://doi.org/10.1021/acs.biomac.2c01505.
40 Wang H, Pu Y, Ragauskas A and Yang B, *Bioresour Technol* **271**:449–461 (2019). https://doi.org/10.1016/j.biortech.2018.09.072.
41 Lisy A, Ház A, Nadányi R, Jablonský M and Šurina I, *Energies* **15**:6213 (2022). https://doi.org/10.3390/en15176213.
42 Thielemans W and Wool RP, *Polym Compos* **26**:694–705 (2005). https://doi.org/10.1002/pc.20141.
43 Zhang N, Zhao M, Liu G, Wang J, Chen Y and Zhang Z, *J Mater Sci* **57**: 8687–8700 (2022). https://doi.org/10.1007/s10853-022-07101-2.

Polymer International published by John Wiley & Sons Ltd on behalf of Society of Chemical Industry.